Int. J. Nano Dimens., 13 (4): 374-386, Autumn 2022

ORIGINAL ARTICLE

PANI modified Ag NPs fluorescence sensor for detection of nitrate ion

Abdu Hussen Ali

Department of Chemistry, College of Natural and Computational Sciences, Mekdela Amba University; P. O. Box 32, Tuluawliya, Ethiopia

Received 16 June 2022; revised 14 July 2022; accepted 24 July 2022; available online 02 August 2022

Abstract

Nitrate is one of the major environmental problems in today's world, which affect human health and welfare, and hinders the sustainable development of both society and the economy. Therefore, the growth of sensor based on decorated noble metal nanoparticles (NPs) such as Ag have been attracted great attention for their convenience of simple operation, excellent absorption and scattering (extinction) properties in recent years. A new and simple fluorometric sensing probe based on polyaniline functionalized AgNPs for NO_{3^-} ion detection was developed by polymerization method. It has been successfully synthesized by in- situ polymerization method. The structural, morphological and optical properties of the as-synthesized nanocomposites were characterized by using, fourier- transform infrared spectroscopy (FT-IR), powder X-ray diffraction (XRD), scanning electron microscopy (SEM) and UV-Vis spectroscopy. In the absence of nitrate ion, the PANI/Ag exhibit high fluorescence intensity. Yet, the strong coordination of the basic sites with nitrate ion causes fluorescence intensities quenching through static quenching leading to the qualitative and quantitative detection of nitrate ion. Factor affecting the detection system such as pH and concentration are optimized. Also, the developed PANI modified Ag sensor exhibits high selectivity and sensitive toward nitrate ion with detection limit of 8.9×10^{-4} M. The practical use of the sensor as well tested by spiked with different concentration of nitrate ion solutions on cabbage samples. The result signposted a good linear relation between FO/F and the spiked concentrations of nitrate ion with coefficient of regression $R^2 = 0.991$ (n= 3) and also confirms that the found values is agreed well with the spiked amount.

Keywords: *Fluorescent Sensor; Nanocomposite; Nitrate Ion; Polyaniline; Quenching; Toxicity.*

How to cite this article

Hussen Ali A. PANI modified Ag NPs fluorescence sensor for detection of nitrate ion . Int. J. Nano Dimens., 2022; 13(4): 374-386.

INTRODUCTION

Chemical pollution is one of the major environmental problems in today's world, since polluted environment poses a threat to human health and welfare, and hinders the sustainable development of both society and the economy. The presence of chemical toxins, heavy metals, inorganic and organic pollutants in water, food and soil, due to either natural or artificial processes result environmental problem [1]. Nitrate is a common chemical compound in the nature, and is widely found in soils, waters, and foods. It has been classified as an inorganic nitrogenous compound, which can cause disease and become a threat to human health. The nitrate can be found naturally in water, soil, and food; thus, it can be easily consumed by humans. Due to the excess of nitrate, symptoms such as abdominal pain and diarrhea have also been observed in human [2] and disruption of endocrine functioning of the thyroid gland are some of the effects of nitrates [3].

Therefore, it needs to be monitored constantly to safeguard the supply of clean drinking water and food to the public, and to control the impact on the environment and the ecosystem. Conventional analytical techniques for nitrate ion detection have been developed, such as ion chromatography

* Corresponding Author Email: *abdelmelik9@gmail.com*

(IC), Raman spectroscopy [4], atomic absorption spectrometry (AAS) [5] and inductively coupled plasma optical emission spectrometry (ICP-OES) [6]. These methods require high-cost analytical instruments developed for use in the laboratories. The necessary sample collection, transportation and pre-treatment is time-consuming and a potential source of error. Recently, the combination of nanotechnology, chemistry, physics and biology, has allowed the development of ultrasensitive detection and imaging methods, including applications in electronic, magnetic, environmental, pharmaceutical, cosmetic, energy, optoelectronic, catalytic, and material fields [7].

The field of environmental monitoring has seen the application of nanoparticles (NPs) being utilized as functional probes for analyzing toxins, metal ions, and inorganic and organic pollutants [8]. NPs, usually with a size between 1 and 100 nm, display unique properties, mainly due to the strong physical confinement of electrons or holes in the NPs at the nanoscale. From a sensing perspective, the small size of NPs gives them large surface-to-volume ratios, which lead to rapid responses and high sensitivity.

In the fields of chemosensors, the organic sensing materials such as conducting polymers [polyaniline (PANI), polypyrrole (PPy), and polythiophene (PTP), etc.] can show response to target analytes at room temperature or low temperature, which has a convenient operating an attractive prospect [9]. It is very attractive in nanoscience and nanotechnology because of their highly π-conjugated polymeric chains and metal like conductivity. Polyaniline (PANI) is unique among conducting polymers due to its chemical and environmental stability, good redox reversibility, tunable electrical conductivity and optical properties. PANI has three different fundamental forms depending on the method employed for the preparation. The only electrically conducting one is the emeraldine salt form (ES: half oxidized), which is the protonated form of PANI-EB [10]. There have been only a few reports on the application of a simple concept that is fluorescence quenching of polyaniline and its derivatives in optical sensor studies; such as Cu/PANI for chloroform [11] and camphor sulfonic acid doped polyaniline for NO_2 and oxygen gas as chemical sensing based on fluorescence quenching were studied [12].

Chemosensors based on decorated noble metal nanoparticles (NPs) have been also attracted great attention for their convenience of simple operation in recent years by virtue of the excellent absorption and scattering (extinction) properties of Ag NPs, which are impossible in its bulk counterparts. The Ag NPs show many advantages, such as higher extinction coefficients, sharper extinction bands, higher ratio of scattering to extinction and extremely high near-field enhancements. However, there were very few reports on Ag NPs for biosensing applications. This is due to the poor chemical stability of Ag NPs as compared with Au NPs. During the past several years, the use of Ag NPs has been increasing with focus on improving the chemical stabilities.

Therefore, in order to improve chemical stability, nanoparticle can also be synthesized by the biological technique which is a remarkable concept known as green synthesis of the nanoparticle. This method is cost-effective, easily available, eco-friendly, less toxic in nature, large-scale production and act as reducing and capping agent as compared to the chemical method which in comparison is very costly along with this it emits hazardous by-product which can have some venomous effect on the environment [13]. Green synthesis of nanoparticles utilizes naturally occupying reducing agent such as plant extract, microorganism, enzymes, a polysaccharide which are simple and viable can act as an alternative to the complex and toxic chemical processes helps to reduce the consequence of chemical methods [14]. Recently, much attention has been given to the high yield production of AgNPs of defined size using various biological systems such as plant extracts. Silver nanoparticles have already been synthesized using various plant extracts such as *Acorus* calamus [15], *Sesuvium portulacastrum* [16], *Ficus carica* [17], *Allophylus cobbe* [18], *Artemisia princeps* [19], and *Typha angustifolia* [20].

In order to improve the chemical stability, in this study, the synthesis of silver nanoparticles has been carried out using the juice extract of well-known and environmentally friend *Citrullus lanatus* (watermelon). The presence of polyphenol in this juice is found to be responsible for the reduction of Ag^{+1} ion to Ag atom and also stabilization of AgNP [21]. Consequently, Ag NPs rapidly gain the popularity. For instance, many groups have started to explore alternative strategies for the development of optical sensors based on their

extraordinary optical properties [22]. In addition, the physical properties of NPs (i.e., optical, electronic, magnetic properties) can be fine-tuned through control of their size, composition, shape, and surface chemistry, to generate highly functional molecular probes. Surface-modified nanoparticles, such as gold and silver NPs (AuNPs/AgNPs) [23], quantum dots (QDs) [24], magnetic NPs (MNPs) [25] and carbon nanotubes [26] can have specific target-binding properties that allow highly selective and sensitive target detection.

In this context, we aimed to establish a new and simple fluorometric sensing probe for NO_3^- detection based on polyaniline functionalized AgNPs. We evaluated the PANI functionalized AgNPs and the prepared PANI functionalized AgNPs tend to form complex with NO_3^-, which leads to the significant emission change spectrum. These results suggest that, the PANI functionalized AgNPs have great potential for applications in fluorescence sensor and optoelectronic devices.

MATERIALS AND METHODS

Materials

Aniline was obtained from Aldrich purified by distillation under reduced pressure prior to use. Sodium dihydrogen phosphate, disodium hydrogen phosphate, hydrochloric acid, Zinc dust, ethanol, ammonium persulphate, Ammonia, Sodium sulphate, Silver nitrate, Sodium bicarbonate , Sodium chloride, Sodium hydroxide, Sodium nitrate were used without purification.

Preparation of juice extract

The *Citrullus lanatus* was collected from local market and washed with distilled de-ionized water. It was cut into pieces. The inner red portion of the pieces was pasted by mortar pestle. Then, it was filtered using whatman filter paper to get *Citrullus lanatus* juice [27].

Synthesis of Nanocomposite

Synthesis of Silver Nanoparticle

Silver nanoparticles was synthesized as follow, 5 mL of double distilled water was added to 5 mL of pure juice extract to make it 1:1 and it was cooled in ice cold water. The solution was made alkaline (pH 10) by adding NaOH. The whole apparatus was placed on a heating mantle. During heating 6 mL 3×10^{-3} M aqueous silver nitrate solution was added drop wise with continuous stirring from burette and finally it was heated for 20 min at 70 °C. The color of the solution gradually changed from light pink to reddish yellow. The reddish yellow color indicated the formation of AgNP [27].

Synthesis of Polyaniline (PANI) Modified Ag NPs

PANI/Ag was synthesized by polymerization of aniline in the presence of AgNPs nanocomposite. 1 g of AgNPs powder was added into 20 mL aqueous solution of 0.01 mol aniline monomer and 0.01 mol hydrochloric acid. A 0.01 mol APS was dissolved in a 15 mL distilled water and then added dropwise to the mixture of AgNPs and aniline with stirring in an ice bath. Polymerization proceeded for 5 h. The composite of PANI modified AgNPs was obtained as a precipitate. The precipitate was isolated by filtration, washed with distilled water and ethanol three times, and dried at 70 °C for 3 h. Pure PANI was also synthesized, by using an identical method but without using AgNPs.

Characterization of the Synthesized Nanocomposites

To determine the characteristic maximum absorption of the as-synthesized samples and their band gaps, UV-Visible absorption spectrophotometer (Shimadzu-1800) was used in the range of 200-900 nm wavelength. The photoluminescence emission properties were determined using a RF-5301PC spectrofluorometer equipped with a xenon discharge lamp. The crystallite sizes were determined using powder X-ray diffraction (XRD) with X'Pert Pro P ANalytical with CuKα radiation (I = 1.5405 Å). The surface morphology was analyzed by SEM-EDX (JSM 6510 LA). The data were registered with 2θ steps of 0.02° and accumulation times of 20 s. FT-IR (Spectrum 65, PerkinElmer) in the range 4000-400 cm^{-1} using KBr pellets was used to assign functional groups of as-synthesized PANI/Ag.

Preparation of Buffers

The 0.1 M phosphate buffer was prepared by weighing approximately 0.8 g of $NaH_2PO_4.2H_2O$ and 6.5180 g of Na_2HPO_4 and dissolving them in water into a 500 mL volumetric flask. It was adjusted using 0.1 M HCl or 0.1 M NaOH to the desired pH. The buffer solution was stored in a fridge at 4 °C [28].

Fluorescence Detection of Nitrate Ion

For fluorescence detection of nitrate ion detection, 1 mg of the PANI/Ag nanocomposite was dissolved in 2.5 mL deionized water and followed

by the addition of different molar concentration of nitrate ion and sonicated. After reaction of 5 min at room temperature, 50 µL of the solution was taken into a cuvette and finally, the emission spectra were recorded using fluorescence spectroscopy.

In order to quantify the nitrate ion induced quenching process, the Stern-Volmer quenching constant K_{SV} was calculated by Stern-Volmer equation:

$$I_O/I = 1+K_{SV}[Q] \quad (1)$$

Where I_O and I are the fluorescence intensities of the sensor in the absence and presence of nitrate ions, K_{SV} is the Stern-Volmer constant and (Q) is the molar concentration of nitrate ion.

Optimization of Parameters

The Effect of Concentration

The effect of nitrate ion concentration also affects the sensitivity of detection. In order to investigate this effect, 2.5 mL of PBS (0.1 M) was added in to 1 mg of the PANI/Ag nanocomposite, then it was dissolved in 2.5 mL deionized water and followed by the addition of 1, 2, 4, 6, 8, 10, 12 and 14 mM of nitrate ion and sonicated. After reaction of 5 min at room temperature, 50 µL of the solution was taken into a cuvette and finally, the emission spectra were recorded using fluorescence spectroscopy.

The Effect of pH

It is common that the pH of a solution can affects the sensitivity and selectivity of a detection. The effect of pH (2-12) of PBS on the PANI/Ag fluorescent sensor in the presence of nitrate ion solution was tested.

Reproducibility and Stability Tests

The reproducibility of the PANI/Ag as the fluorescent sensor was investigated at three repetitions on three batches of the PANI/Ag. A calibration graph was for mean of F_O/F, (F_O and F represented the fluorescence intensity of sensor without and with nitrate ion) Vs. nitrate ion concentration, which a linear range was then determined. Limit of detection was calculated using the following formula;

$$LOD = \quad (2)$$

Where LOD are limit of detection, SD are standard deviation from linearity of a graph and K_{SV} is Stern-Volmer constant calculated from the graph [29].

Selectivity of the Sensor

The SO_4^{2-}, Cl^-, OH^- and HCO_3^- ions were used to investigate selectivity for nitrate ion of PANI/Ag sensor. The concentration of each anion was 14 mM. The same detection conditions and approach were used as mentioned above.

Recovery Test and Real Samples Analysis

About 5 g of cabbage sample was collected from the local market, Tuluawliya, Ethiopia for nitrate extraction. The cabbage was torn into very small pieces and ground using pistol and mortar. The powder was added into a flask that contains 20 mL of ethanol and sonicated for 15 minutes. The mixture was filtered through a Buchner funnel to separate the liquid from the solid plant material and the liquid part was diluted by adding 5 mL of deionized water. The resultant samples were spiked with different concentrations of nitrate solutions. Then 200 µL of this sample solution was taken and added to PANI/Ag nanocomposite in 2.5 mL deionized water. Finally, fluorescence emission spectra were recorded after reaction of 5 min at room temperature. The mean percentage recoveries for the nitrate ions were calculated using the following equation:

$$\text{Percentage recovery} = \frac{CE}{CM}\text{X}100 \quad (3)$$

Where CE is the experimental concentrations determined from the calibration curve and CM is the spiked concentrations.

RESULTS AND DISCUSSION

Characterization of Modified Ag sensor

FTIR Analysis

Fig. 1 displayed that, the FT-IR spectra of the synthesized nanocomposite samples Polyaniline, Ag NPs and PANI/Ag, in the range 4000-400 cm^{-1} using KBr pellets. Fig. 1(a) shows the FTIR spectra of emeraldine salt PANI. The characteristics peaks are 3435 cm^{-1} due to N-H stretching mode, 1595 cm^{-1} due to C=C stretching mode of the quinoid rings, 1384 cm^{-1} due to C=C stretching mode of benzenoid rings, 1250 cm^{-1} due to C–N stretching mode and 1120 cm^{-1} due to N=Q=N, where Q represents the quinoid ring [30]. The presence of the benzenoid and quinoid units is evidence of the

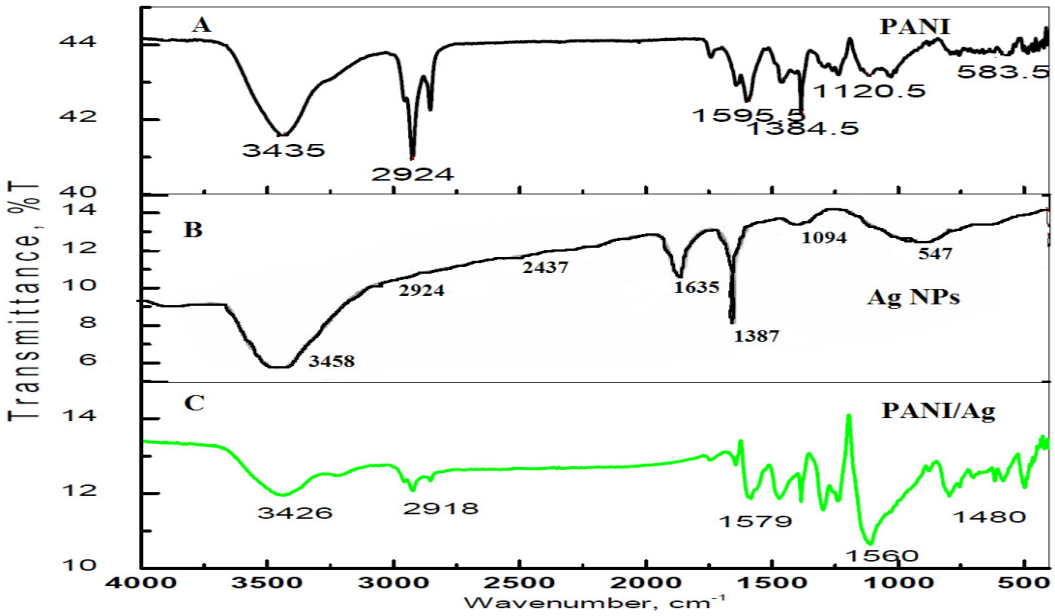

Fig. 1. FT-IR spectra of PANI/Ag nanocomposite.

emeraldine salt form of PANI. For AgNP the FTIR spectra is described in Fig. 1 B. The spectrum shows slightly narrower peak at 3458 cm^{-1} which may be due to hydroxyl (OH) stretching bands which suggests the involvement of the polyphenols in the reduction [31]. The peak at 1635 cm^{-1} may be due to the presence of carbonyl group (C = O) associated with NH moiety in Riboflavin.

The FTIR spectra of PANI/Ag nanocomposite described in Fig. 1C, which shows a peak at 3426 cm^{-1} are attributed to N-H stretching mode because the range of N-H is between 3300 cm^{-1} to 3500 cm^{-1} for amine part of PANI and also due to hydroxyl (OH) stretching bands polyphenols of AgNPs. The small absorption peaks observed at 2918 cm^{-1} and 2850 cm^{-1} are due to asymmetric C-H and symmetric C-H stretching vibrations. Most of the observed characteristic peaks of PANI/Ag nanocomposite is the replica of characteristic peaks of PANI. However, the corresponding peaks are shifted to the lower wave numbers, besides their intensities are changed after the Ag nanoparticles addition. The peaks of the PANI around 3435, 1595, 1384 and 1120 cm^{-1} are shifted to 3426, 1579, 1250 and 1080 cm^{-1}, respectively. These shifts of characteristic peaks of the PANI may be the result of the interactions between the PANI chains and Ag nanoparticles which affect the electron densities and bond energies of the PANI [32]. The shifting to the lower wave numbers is due to the action of hydrogen bonding between the hydroxyl groups on the surface of Ag nanoparticles and the amine groups in the PANI molecular chains. The characteristic band at 810 cm^{-1} is corresponding to out-of-plane bending vibration of C–H bond of *p*-disubstituted benzene rings of PANI [33] which confirm that coupling of aniline unit in the surface of AgNPs.

XRD Analysis

Fig. 2a describe the XRD analysis of biosynthesized AgNP to confirm the crystalline nature. From the figure, it shows a major characteristics peak at 38.20°, 44.10°, 46.87°, 64.59° and 80.80°. corresponding to the (111), (200), (220), (311) and (222) crystallographic planes [JCPDS No. 04-0783], respectively. The other peaks are 31.81°, 46.87°, 55.2° and 57.8°. The result indicate that the synthesized AgNP is crystalline and essentially fcc in nature. This result is a good agreement with other works Ag synthesis extracted from plant material [27]. For pure PANI, Fig. 2B shows the XRD pattern revealed three weak peaks observed at 2θ values of 15.1°, 20.53° and 25.36° corresponding to (111), (100) and (011) plane, which can be attributed to the

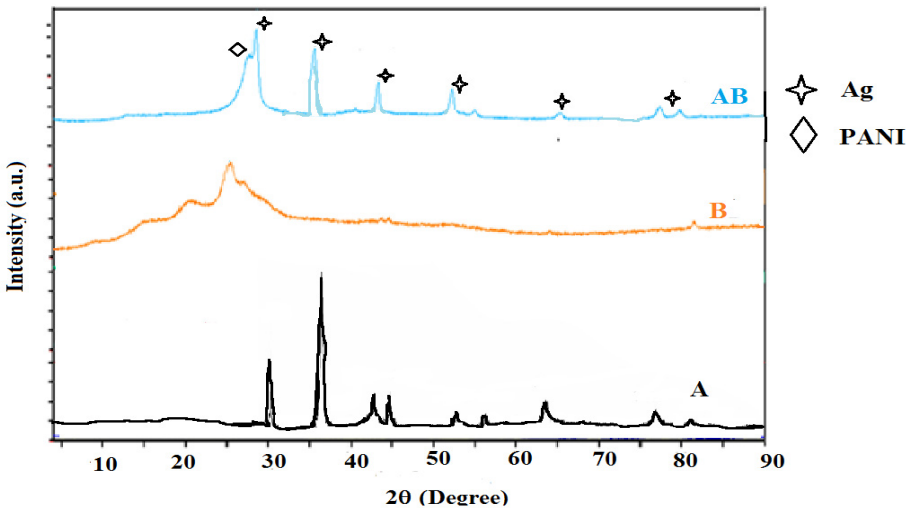

Fig. 2. XRD patterns of the as-synthesized nanocomposites (where a: Ag NPs, b: PANI, ab: PANI/Ag).

Table 1. The full width at half maximum (in radian) and crystal sizes of as-synthesized sensor.

Samples	θ (radian)	β (radian)	Average crystal size (nm)
AgNPs (A)	0.785	0.0078	22.69
PANI (B)	0.903	0.0039	39.34
PANI/AgNPs (AB)	0.88	0.014	11.24

crystallographic planes for the emeraldine salt form of PANI, which is in a good agreement with other report [34]. The peak at 15.1° is attributed to parallel repeat units of PANI, as well as the peak at 25.36° is assigned to a periodicity caused by H-bonding between PANI chains. The low intensity of the observed peak indicates that the PANI has semi-crystalline nature due to the presence of a benzenoid and quinonoid group [35].

The XRD diffraction of PANI/Ag nanocomposite consist of the major characteristic's diffraction peak of PANI and Ag, yet however the 2θ values of the peaks slightly shifted. The diffraction peak observed at 2θ values of 28.27^o could be attributed to PANI and 32.15°, 39.0°, 45.43°, 65.34° and 78.58° could be due to AgNP. The increase in the degree of regularity is due to the strong interfacial interaction between the PANI and AgNP.

The average crystalline sizes (D) of all the five as-synthesized nanocomposites were calculated using the Debye-Scherrer's equation.

$$D = \frac{k}{\beta \cos\theta} \quad (4)$$

Where D is the mean crystallite dimension in nm, K is the crystallite shape factor constant (0.9), q the Bragg angle in radians, l is the wavelength of X-ray (0.15406 nm), and b the full width at half maximum (FWHM) of the peak in radians. Table 1 depicts the calculated values of crystalline size of as-synthesized sensor labelled as A, B, and AB for Ag, PANI, and PANI/AgNPs which is 22.69 nm, 39.3 nm and 11.24 nm respectively. The result indicated that the average crystal size of all as-synthesized nanocomposite was in nano rage. The average crystalline size of PANI/AgNPs was less than the single nanoparticle, this indicates the nanocomposite has large surface area.

Morphological Analysis (SEM)

Surface morphology and shape of the synthesized nanomaterial was analyzed by scanning electron microscopy as described in Fig. 3. The SEM image of pure silver nanoparticles by using fruit extract of *Citrullus lanatus* (Watermeline), the surface morphology exhibited even shape and spherical nature. Thus, the result indicated *Citrullus lanatus* extract acts as a strong reducing and capping agent in the assembling

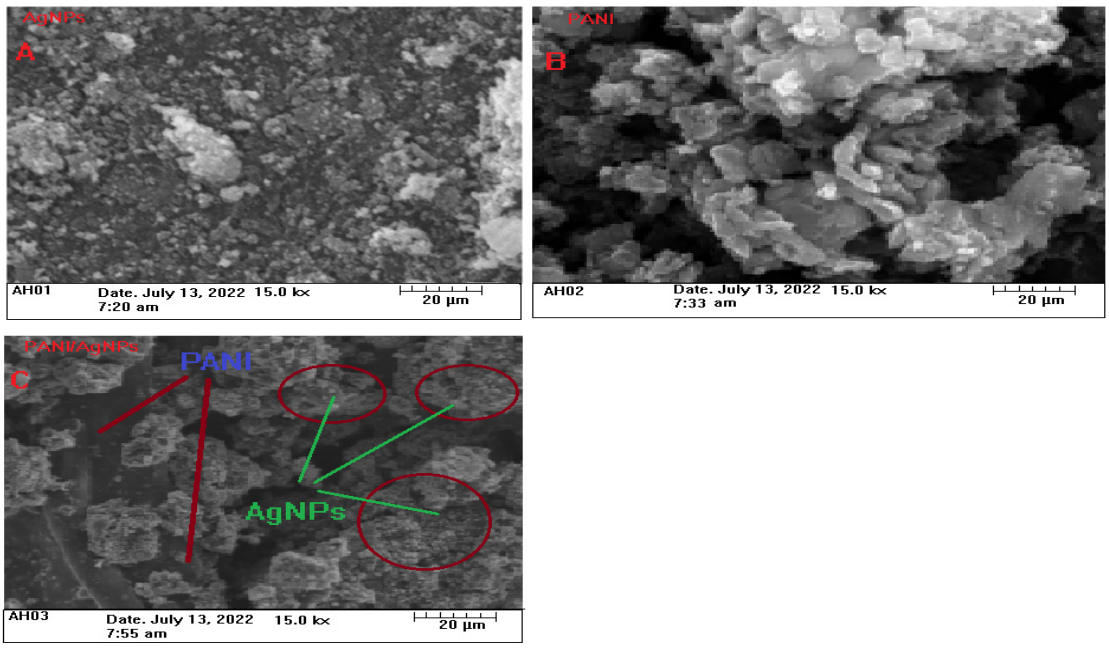

Fig. 3. SEM Analysis of the synthesized nanomaterial **(where a: Ag NPs, b: PANI, ab: PANI/Ag).**

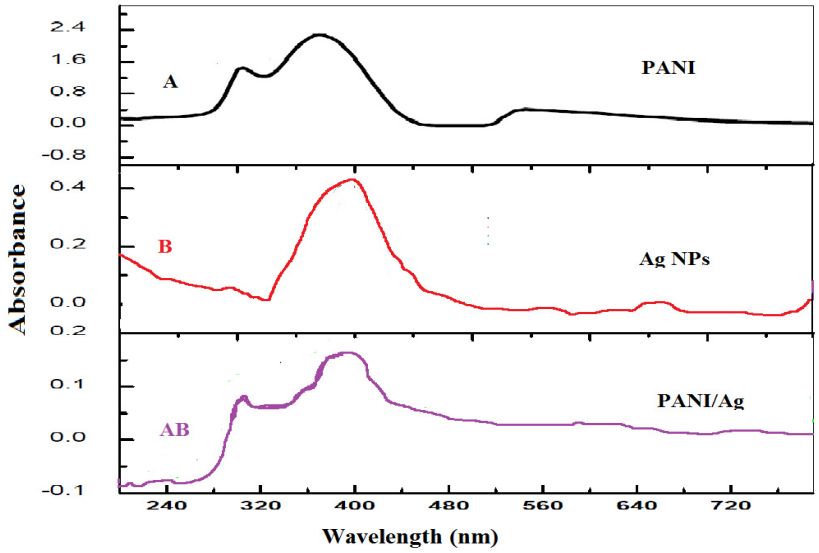

Fig. 4. UV–vis DRS analysis of the as-synthesized composites.

of silver nanoparticles. The morphology of pure PANI shows flake structure since PANI has various structure such as granules, nanofiber, nanotubes, nanosphere, microspheres and flake. Whereas the SEM analysis of PANI/AgNPs, the Ag particle are clearly agglomerate and embedded on the surface of the polyaniline (PANI). This due by hydrogen bonds that occur due to the interaction between Ag and N-H groups.

UV-Visisble Analysis

The absorbance spectrum of samples of PANI showed the absorption peaks at 290 nm assigned to the benzenoid structure and 380 nm which indicate the principal absorption of the π-π* orbital transitions of the emeraldine form of PANI (Fig. 4a) as similar with previously investigated [36], almost under similar conditions. PANI can absorb both UV and visible region due to

transitions in the PANI molecules. The absorption reveals maximum at about 380 and 550 nm, which originate from the charge transfer excitation from the HOMO level to the LUMO energy level and the π–π* transition [37]. The second peak at 380 nm which also indicates the presence of benzenoid group and lone pair of electrons of nitrogen. This, in turn, leads to π-π* interactions of the molecule and this shows that it is a conducting polymer. For AgNPs a broad absorption band was observed at 405 nm (Fig. 4B). As the sharp, single peak represents the monodispersity of the extract and water composition.

The UV-Visible spectra of PANI/Ag nanocomposite also show a sharp peak at 280 nm (Fig. 4ab) may be assigned to the localized polaron which are characteristics of the protonated PANI, together with extended conducting emeraldine salt form of the sample. The absorption peak red-shifted to the resultant PANI/Ag hybrids suggesting that the recovery of electronic conjugation within the polyaniline occurred. Additionally, the absorption exhibited in the visible region has small absorption peaks at 280 nm, which might be in the relation of the more conductivity of the nanocomposite with the porous of PANI and the peaks at 400 nm specifically indicate the presence of Ag NPs on the surface of PANI.

Mechanism of the Modified Ag Fluorescent Sensor for Nitrate Ion

PANI modified AgNPs exhibited characteristic strong absorption band respectively at 440 nm, and reddish-yellow color in aqueous solution that confirms the formation of AgNPs. The emission intensities of the PANI/Ag nanocomposite were quenched after addition of the nitrate ion. The decrease in the emission intensity can be attributed to the combined effect of decrease in absorbance at the excitation wavelength and due to complex formation between the NO_3^- and PANI/Ag. Therefore, the quencher probably involves the donation of electrons from the surface of PANI/Ag nanomaterial to the nitrate ion, deactivating the excited state responsible for fluorescence quenching.

The other possibility for fluorescence intensity quenching occurs due to the most possible interactions between Ag and N sites in PANI/Ag with nitrate ion would be non-covalent interaction like electrostatic or hydrogen bond for chelation (NH/ N-O and Ag-O-N). In addition, the nitrogen-containing groups (nitrogen site) in the PANI/Ag and nitrate ion might be reacted to produce N-nitroso compounds, which results in fluorescence static quenching. This indicates that fluorescence quenching is caused by chemical reactions. The mechanism of quenching at low nitrate ion concentrations may also mostly involves dynamic quenching, which results from collisions between nitrate ions and the PANI/Ag NPs. Static quenching also occurs, but only at higher concentrations.

Optimization of Experimental Conditions

In order to evaluate the sensitivity of the proposed material, the experimental conditions were optimized including the pH of the buffer solution and concentration of nitrate ion.

The Concentration of Nitrate Ion

For detection of NO_3^- ion present in aqueous solution, coordination complex formation method has been tried and consequent emission intensities changes have been perceived. Several concentrations (0–14 mM) of NO_3^- solutions were used for the purpose of complex formation. As displayed in Fig. 5, the intensities of the emission spectra of the PANI/Ag were found to decrease with the addition of nitrate ion. The decrease in intensities indicated that the sensor sites excited at the specific excitation wavelengths interacted with NO_3^- molecule and the interactions led to the decrease in the emission intensity. In addition, the red shifting of the excitation spectra at low concentration may be due to electron density changes caused by the complexation of NO_3^- and a conformational change in the sensor backbone as a result of the chelation. The emission intensity of the PANI/Ag was found to decrease as the concentration of the NO_3^- increased up to 14 mM. More increase in the concentration of NO_3^- did not cause a further decrease in the emission intensity. This indicate that of the all interaction sites of the sensor are occupied by NO_3^- molecules. Therefore, has no sites to interact with additional NO_3^- ion. From this data 14 mM of nitrate ion was optimum concentration.

Influence of pH

The influence of pH on the quenching emission intensity of PANI/Ag by nitrate ion was described in Fig. 6 below. The PANI/AgNPs showed significant notice-able effects with the change in pH. The

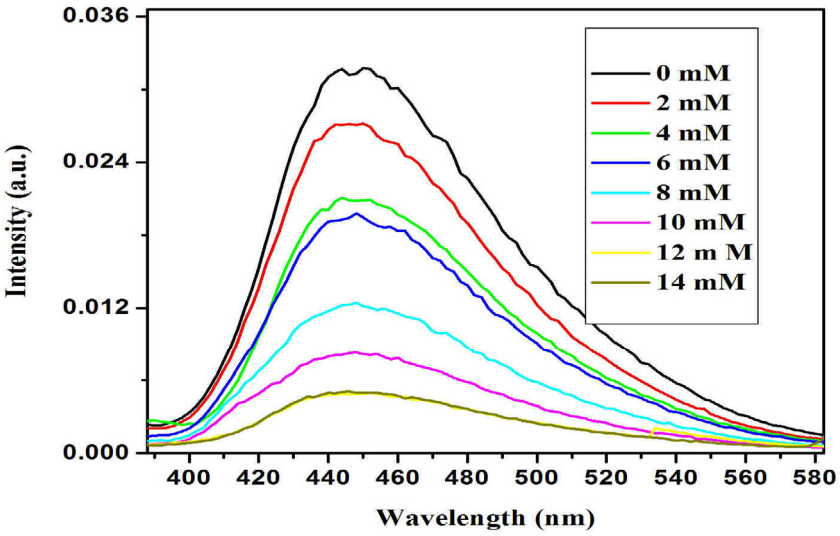

Fig. 5. Emission spectrum of PANI/Ag upon addition of NO_3^- ion with various concentration.

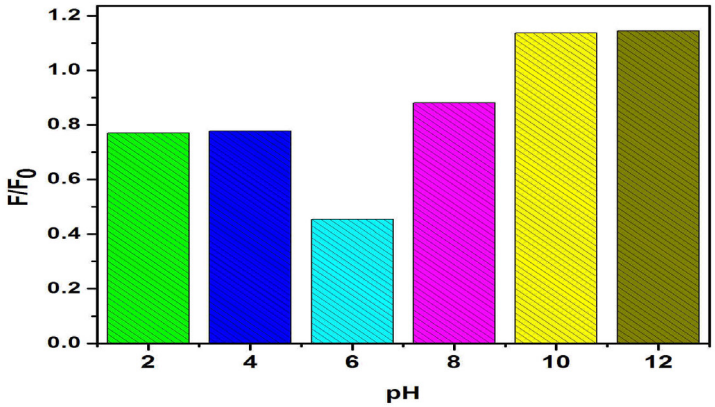

Fig. 6. Effect of pH (2-12) on emission spectrum of PANI/Ag upon addition of NO_3^- ion.

shift to lower intensity, as well as the relative intensity ratio values decrease on going from pH 2 to pH 4. This is due to the complexation of NO_3^- ions hindered because the necessary lone pair electrons are occupied by protons thereby week interaction persists, resulting in a low quenching efficiency.

As the pH increased, the fluorescence intensity significantly decreased due to the high quenching efficiency and maximum quenching was observed at pH 6. This is due to the deprotonation of the interaction site, which increases the covalent bond strength between the sensor and nitrate ion. As the pH further increases for basic condition, since competitive metal hydroxide formation, it resulted in a distinct increase in fluorescence intensity resulting in a poor interaction with the sensor. Therefore, pH 6 is recommended as the optimal pH value for further detection.

The Sensitivity of the Detection System

Under the above optimal conditions, the fluorescence intensity of PANI/Ag was found to be such that quenching and the Stern-Volmer fluorescence intensity ratio (F_O/F) show a linear diminish with the increasing the nitrate ion is also linearly related with a concentration of 1-14 mM as shown in Fig. 7. The experiments showed that the nitrate ion concentration is inversely proportional to fluorescence intensity, and gave a good linear change in Stern-Volmer fluorescence emission intensity ratio. In order to clarify the favorable condition for the PANI/Ag to interact with the nitrate ion molecules, quenching efficiency at

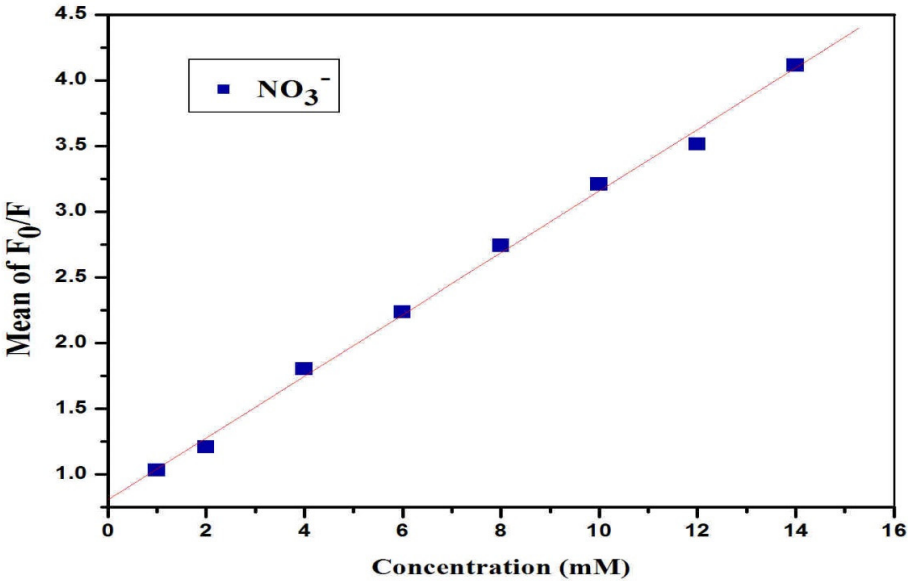

Fig. 7. The reproducibility of the PANI/Ag responses for NO_3^- ion concentration.

Table 2. Detection of nitrate ion in cabbage samples by spiked method (n = 3).

Samples	Added (mM)	Found (mM)	Mean recovery (%) [a]	RSD (%)
1	1	1.032	103.2	1.04
2	6	5.41	90.1	2.7
3	12	12.26	102.1	4.2

Table 3. Comparison of sensing performance PANI/Ag towards NO_3^- with another fluorophore.

Sensing material	**Linear range**	**LOD (M)**	**Reference**
EDTA-AgNPs	0 -2.5 µgmL^{-1}	1.8 x 10^{-4}	[38]
CN	0 -1800 µM	2.61 x 10^{-7}	[39]
GO	0-10 mM	-	[40]
PANI/Ag	0-14 mM	8.9 x 10^{-4}	**This work**

excitation wavelength was determined using a Stern-Volmer plot (eqn 1).

In a fluorescent sensor, the emission intensity ratio can be defined as the response of the sensor. The sensing capability of the PANI/Ag was revealed from the slopes of the linear plots, which were corresponding to the quenching rate constants (K_{SV}). From the calibration curve, it can be described that the linear dependence of the emission intensity on the concentration of nitrate ion. A linear relationship with the coefficients of regression of 0.996. The calculated K_{SV} value for the PANI/Ag fluorescent sensor for detection of nitrate ion was found to be 2.22×10^2 M^{-1}.

In order to determine the limit of detection of the sensor, the reproducibility of the PANI/Ag at the linear range was investigated at three repetitions. As Fig. 7 shows the reproducibility of the PANI/Ag sensor for each concentration of nitrate ions. The LOD of the sensor for nitrate ion determined from the standard deviation of the response at the intercept of the regression line and the value of the K_{SV} (eqn 2). The limit of detection of the proposed fluorescent sensor for nitrate ion were found to be 8.9 x 10 $^{-4}$ M. The detection limit in this case was also good compared with those of the other fluorophore based fluorescent sensing methods as described in Table 3.

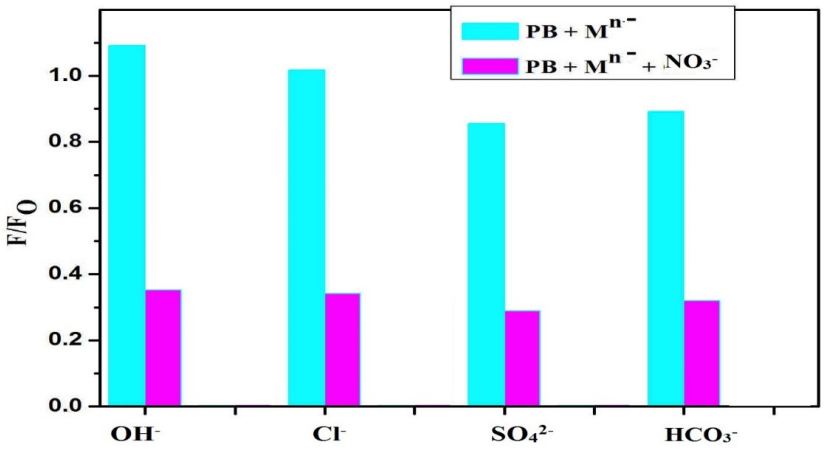

Fig. 8. Fluorescence responses of PB = PANI/Ag (left bar) after treatment of 14 mM NO_3^- ion solutions, and interference of 14 mM of other anions with 14 mM NO_3^- ion (right bar).

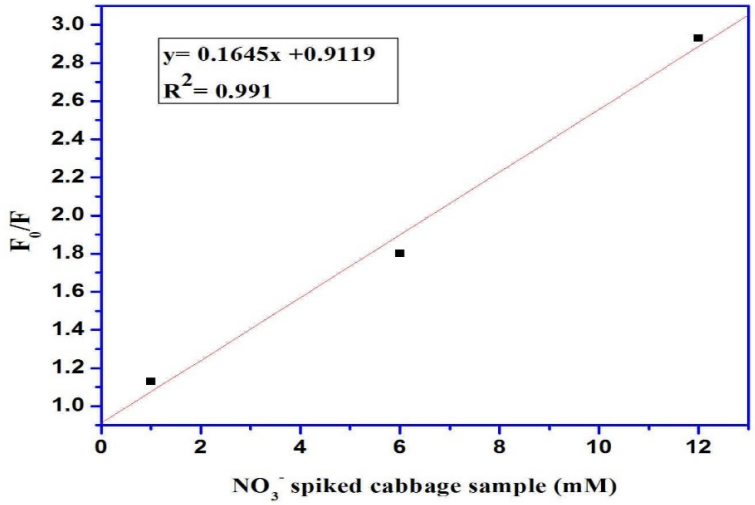

Fig. 9. Calibration curve of F_0/F Vs. different concentration of nitrate ion spiked samples.

Selectivity Test

The selectivity of PANI/Ag for nitrate ion detection was performed by adding the same amount of interferents (SO_4^{2-}, HCO_3^-, Cl^- and OH^-) into the system. The extent of interference for each anion was shown in Fig. 8. This result confirms that the detection of nitrate ion by PANI/Ag fluorescent sensor were mostly not influenced by the above interference ions. However, the co-existence of polyatomic anions such as SO_4^{2-} and HCO_3^- resulted in higher efficiency than other. Therefore, the sensing performance would be slightly affected in the presence of these ions.

Recovery test

The cabbage samples were spiked with different concentration of nitrate ion solutions. By using the calibration curves plotted for the known standard solution (spiked) of nitrate ion, the unknown (found) concentration of nitrate ion (value of X) was successfully calculated by using equation y = A + B*X obtained from the calibration curves of the standard solution. Therefore, the value of "A" is intercept and B (slope) and the value of y (F_0/F) was obtained from the fluorescence recorded for nitrate ion for respective samples. The result indicated a good linear relation between

F_O/F and the spiked concentrations of nitrate ion with coefficient of regression R^2 = 0.991 (n= 3), respectively as described in Fig. 9 below. The result confirms that the found values is agreed well with the spiked amount. The obtained recoveries were summarized in Table 2 below, which demonstrates that the proposed method is valid and denoting no serious interferences in the samples. In addition, the RSD were less than 5 %, suggesting a high precision of the proposed method.

CONCLUSION

In these study, green synthesis of the nanoparticle from plant extract shows cost-effective, easily available, eco-friendly, and less toxic in nature. The a new and simple PANI/Ag fluorometric sensing probe for NO_3^- detection has been successfully synthesized by polymerization of polyaniline into the surface of Ag NPs. The prepared materials were characterized by using FT-IR, XRD SEM, and UV-Visible spectroscopy. The results of the analysis indicated that there is a strong interfacial interaction between polyaniline and Ag NPs. The developed sensor employed as a highly effective tool for selective detection of NO_3^- ions present in aqueous solution was based on quenching in the emission intensities resulting from complex formation of the sensor molecule with nitrate ion. The effect approves, the nitrate ion effectively quenched the emission and excitation intensity of PANI/Ag. The dynamic and static quenching mechanisms are show a significant role in the interaction of nitrate ion with the sensing sites of the developed sensor. The developed PANI decorated Ag NPs have their suitability of simple operation and distinct types of optical responses observed, that is due to high surface-area-to-volume ratio. The sensor revealed a linear range, a high selectivity and sensitivity with K_{SV} of 2.22×10^2 M^{-1}. The practical use of the sensor also tested by using cabbage sample and shows a good sensitivity.

CONFLICTS OF INTEREST

The authors do not have any conflicts of interest.

REFERECES

[1] Wang L., Ma W., Xu L., Chen W., Zhu Y., Xu C., Kotov N. A., (2010), Nanoparticle- based environmental sensors. *Mater. Sci. Eng.* 70: 265 – 274.

[2] Namasivayam C., Sageetha D., (2005), Removal and recovery of nitrate from water by $ZnCl_2$ activated carbon from coconut coir pith, and agricultural solid waste. *Indian J. Chem. Technol.* 12: 513- 521.

[3] Braverman L.E., He X., Pino S., Cross M., Magnani B., Lamm S.H., Kruse M. B., Engel A., Crump K. S., Gibbs J. P., (2005), The effect of perchlorate, thiocyanate, and nitrate on thyroid function in workers exposed to perchlorate long-term. *J. Clin. Endocrinol. Met.* 90: 700-706.

[4] Niedzielski P., Kurzyca I., Siepak J., (2006), A new tool for inorganic nitrogen speciation study: Simultaneous determination of ammonium ion, nitrite and nitrate by ion chromatography with post-column ammonium derivatization by Nessler reagent and diode-array detection in rain water samples. *Anal. Chim. Acta*. 577: 220-224.

[5] Pourreza N., Hoveizavi R., (2005), Simultaneous preconcentration of Cu, Fe and Pb as methylthymol blue complexes on naphthalene adsorbent and flame atomic absorption determination. *Anal. Chim. Acta*. 549: 124–128.

[6] Chaiyo S., Chailapakul O., Sakai T., Teshima N., Siangproh W., (2013), Highly sensitive determination of trace copper in food by adsorptive stripping voltammetry in the presence of 1, 10-phenanthroline. *Talanta*. 108: 1- 6.

[7] Auffan M., Rose J., Bottero J. Y., Lowry G. V., Jolivet J. P., Wiesner M. R., (2009), Towards a definition of inorganic nanoparticles from an environmental, health and safety perspective. *National Nanotechnol*. 4: 634 – 641.

[8] Wang Z., Ma L., (2009), Gold nanoparticle probes. *Coord. Chem. Rev.* 253: 1607 – 1618.

[9] Ma X. F., Mang W., Li G., Chen H. Z., Bai R., (2006), Preparation of polyaniline-TiO_2 composite film with in situ polymerization approach and its gas-sensitivity at room temperature. *Mater. Chem. Phys.* 98: 241-247.

[10] Masoumi V., Mohammadi A., Amini M., Khoshayand M. R., Dinarvand R., (2014), Electrochemical synthesis and characterization of solid-phase microextraction fibers using conductive polymers: application in extraction of benzaldehyde from aqueous solution. *J. Solid State Electrochem*. 18: 1763-1771.

[11] Sharma S., Nirkhe C., Pethkar S., Athawale A. A., (2002), Chloroform vapour sensor based on copper/polyaniline nanocomposite. *Sens. Actuators B. Chem*. 85: 131-136.

[12] Draman S. F. S., Daik R., Musa A., (2009), Synthesis and studies on fluorescence spectroscopy of CSA-doped polyaniline solution in DMF when exposed to oxygen gas. *Malays. Polym. J.* 4: 7-18.

[13] Pramila M., Meenakshisundaram M., (2017), Biosynthesis of iron (Fe) nanoparticles and its inhibitory effect on *Pseudomonas Aeruginosa* biofilm. *Indian J. App. Res*. 7: 251- 524.

[14] Das R. K., Pachapur V. L., Lonappa L., Naghdi M., Pulicharla R., Maiti S., (2017), Biological synthesis of metallic nanoparticles: Plants, animals and microbial aspects. *Nanotechnol. Environ. Eng.* 18: 1-21.

[15] Nakkala J. R., Mata R., Gupta A. K., Sadras S. R., (2014), Biological activities of green silver nanoparticles synthesized with *Acorous calamus* rhizome extract. *Eur. J. Med. Chem.* 8: 784-794.

[16] Nabikhan A., Kandasamy K., Raj A., Alikunhi N. M., (2010), Synthesis of antimicrobial silver nanoparticles by callus and leaf extracts from saltmarsh plant *Sesuvium portulacastrum* L, Colloid. *Surface. B.* 79: 488-493.

[17] Ulug B., Turkdemir M. H., Cicek A., Mete A., (2015), Role

of irradiation in the green synthesis of silver nanoparticles. *Spectrochim. Acta A*. 135: 153-161.

[18] Gurunathan S., Han J., Park J. H., Kim J. H., (2014), A green chemistry approach for synthesizing biocompatible gold nanoparticles. *Nanoscale Res. Lett*. 9: 248-253.

[19] Gurunathan S., Jeong J. K., Han J. W., Zhang, X. F., Park J. H., Kim J. H., (2015), Multidimensional effects of biologically synthesized silver nanoparticles in Helicobacter pylori, Helicobacter felis, and human lung (L_{132}) and lung carcinoma A_{549} cells. *Nanoscale Res. Lett.* 10: 1–17.

[20] Gurunathan S., (2015), Biologically synthesized silver nanoparticles enhance antibiotic activity against Gram-negative bacteria. *J. Ind. Eng. Chem.* 29: 217–226.

[21] Maiti S., Barman G., Konar L. J., (2014), Biosynthesized Gold nanoparticles as catalyst. *Int. J. Sci. Eng. Res.* 5: 1229–1230.

[22] Misra T. K., Liu C. Y., (2009), Surface-functionalization of spherical silver nanoparticleswith macrocyclic polyammonium cations and their potential for sensing phos-phates. *J. Nanoparticle Res.* 11: 1053–1063.

[23] Wang Q., Yu C., (2009), Chemical and biological sensing and imaging using plasmonic nanoparticles and nanostructures. *Biomed. Nanosens.* 2012: 59–96.

[24] Qu L. H., Peng Z. A., Peng X. G., (2001), Alternative routes toward high quality CdSe nanocrystals. *Nano Lett.* 1: 333–337.

[25] Koh I., Hong R., Weissleder R., Josephson L., (2008), Sensitive NMR sensors detect antibodies to influenza. *Angew. Chem. Int. Ed. Engl*. 47: 4119–4121.

[26] Zhang J., Lei J., Xu C., Ding L., Ju H., (2010), Carbon nanohorn sensitized electrochemical immunosensor for rapid detection of microcystin-LR. *Anal. Chem*. 82: 1117–1122.

[27] Maiti S., Barman G., Konar Laha J., (2016), Detection of heavy metals (Cu^{+2}, Hg^{+2}) by biosynthesized silver nanoparticles. *Appl. Nano. Sci*. 6: 529–538.

[28] Bisetty K., Sabela M. I., Khulu S., Xhakaza M., Ramsarup L., (2011), Multivariate optimization of voltammetric parameters for the determination of total polyphenolic content in wine samples using an immobilized biosensor. *Int. J. Electro. Chem. Sci.* 6: 3631-3643.

[29] Alim N. S., Lintang H. O., Yuliati L., (2015), Fabricated metal-free carbon nitride characterizations for fluorescence chemical sensor of nitrate ions. *J. Eng. Sci. Technol.* 76: 1-6.

[30] Silva R. F., Zaniquelli M. E. D., (2002), Morphology of nanometric size particulate aluminium-doped zinc oxide films. *Colloids Surf. A*. 551: 198-203.

[31] Song J. Y., Jang H. K., Kim B. S., (2009), Biological synthesis of gold nanoparticles using Magnolia kobus and Diospyros kaki leaf extracts. *Process Bio. Chem.* 44: 1133–1138.

[32] Niu Z., Yang Z., Hu Z., Lu Y., Han C. C., (2003), Polyaniline-Silica composite conductive capsules and hollow spheres. *Adv. Funct. Mater.* 13: 949-954.

[33] Ayad M. M., Salahuddin N. A., Minisy I. M., Amer W. A., (2014), Chitosan/ polyaniline nanofibers coating on the quartz crystal microbalance electrode for gas sensing. *Sens. Actuators B*. 202: 144-153.

[34] Sonker R. K., Yadav B. C., (2017), Development of Fe_2O_3–PANI nanocomposite thin film based sensor for NO_2 detection. *J. Taiwan Inst. Chem. Eng*. 77: 276-281.

[35] Gu L., Wang J., Qi R., Wang X., Xu P., Han X., (2012), A novel incorporating style of polyaniline/TiO_2 composites as effective visible photocatalysts. *J. Mol. Catal. A. Chem*. 357: 19-25.

[36] Melaku W., Yadav, O. P., Kebede T., (2014), Photo-catalytic removal of methyl orange dye by polyaniline modified ZnO using visible radiation. *Sci. Technol. Art. Res. J*. 3: 93-102.

[37] Singh S., Rama N., Rao M. S. R., (2006), Influence of d–d transition bands on electrical resistivity in Ni doped polycrystalline ZnO. *Appl. Phys. Lett.* 88: 222111-222113.

[38] Wang C. C., Luconi M. O., Masi A. N., Fernández L. P., (2009), Derivatized silver nanoparticles as sensor for ultra-trace nitrate determination based on light scattering phenomenon. *Talanta*. 77: 1238-1243.

[39] Tang H., Sundari R., Lintang H. O., Yuliati L., (2016), Detection of nitrite and nitrate ions in water by graphene oxide as a potential fluorescence sensor. *IOP Conf. Ser.: Mater. Sci. Eng.* 107: 012027-012033.